Jestr

Journal of Engineering Science and Technology Review 17 (2) (2024) 157 - 164

Research Article

JOURNAL OF
Engineering Science and Technology Review

www.jestr.org

Parameter Identification of Nonlinear Flux-Linkage Model for Switched Reluctance Motor Based on Chaotic Diagonal Recurrent Neural Network

Libiao Wang[1,*], Koudjou Takam Lionel[1], Ping Chen[2] and Lianghui Yang[3]

[1]*College of Intelligent Manufacture, Taizhou University, Taizhou 318000, China*
[2]*Lvmei Pumps Co.,Ltd., Wenling 317500, China*
[3]*Wenling Research Institute of Taizhou University, Wenling 317500, China*

Received 12 January 2024; Accepted 26 April 2024

Abstract

Given the high saturation, strong nonlinearity, and tight coupling characteristics of the magnetic paths in a switched reluctance motor (SRM), accurately modeling flux-linkage is challenging, thus leading to excessive torque ripple during SRM torque control. In order to enhance the precision of the SRM flux-linkage model, a neural network-based method for the parameter identification of SRM's nonlinear flux-linkage model was proposed in this study. Logistic mapping elements were incorporated into the feedback layer of the diagonal recurrent neural network (DRNN), and chaotic control parameters were designed. Then, the construction of an analytical model of the nonlinear exponential flux-linkage function using the chaotic diagonal recurrent neural network (CDRNN) was established. By utilizing sample data of flux-linkage, current, and angular position, the parameters of this model were estimated, thus achieving a precise nonlinear exponential function model of the flux-linkage. Results show that, the integration of logistic mapping in the CDRNN feedback layer effectively prevents the local minima typically associated with conventional DRNN. The maximum error in the identified flux-linkage is less than 0.01 *Wb*, and the accuracy reached 95%. Compared with the DRNN method, the CDRNN approach demonstrates significantly reduced errors and higher model precision. This study offers valuable insights for enhancing the performance of SRM torque ripple control.

Keywords: Switched reluctance motor, Flux-linkage model, Neural network, Nonlinear modeling

1. Introduction

In the context of sustainable development strategies, motor drive systems powered by electricity have shown extensive potential in new energy vehicles, aerospace, and other sectors. However, complex working environments have imposed demands for high efficiency, high power density, wide speed regulation ranges, and high reliability [1, 2]. Among the various motor drive technologies, the switched reluctance motor drive system (SRD) offers significant advantages, including high startup torque, low startup current, numerous controllable parameters, flexible and convenient control, and no risk of direct short-circuiting [3]. The switched reluctance motor (SRM), which is the core component of the SRD, is characterized by a simple structure where the rotor is composed of silicon steel sheets with high magnetic permeability, along with concentrated windings on the stator and no permanent magnetic materials. Functionally, the SRM operates independently in each phase, thus ensuring that a single- phase fault does not affect the operation of other phases [4, 5]. These advantages make the SRM particularly suitable for harsh operational conditions, such as high speed, high temperature, and an environment requiring frequent start and reversal. Despite their benefits, the magnetic saturation and nonlinearity of SRM result in significant torque ripple. This outcome adversely affects performance, especially in applications with low rotational inertia where torque ripple can cause noticeable speed fluctuation, thus limiting further industrial application and development of SRM [6].

To meet the high-performance and high-precision requirements of these specific applications, reducing SRM torque ripple through optimized control algorithms has become a focal point of research. Establishing an accurate SRM model is fundamental for analyzing and predicting motor performance and suppressing motor torque ripple. The SRM model primarily includes flux-linkage and torque models, with the torque model being derivable from the flux-linkage model. Thus, flux-linkage modeling is key to SRM nonlinear modeling [7]. Given SRM's unique double-salient pole structure and the principle of "minimum magnetic reluctance" operation, its magnetic inductance and other parameters exhibit high nonlinearity with respect to current and rotor position. This highly nonlinear relationship complicates the magnetic path with high saturation and strong coupling, thus posing significant challenges in developing accurate flux-linkage models for SRM [8].

In response, scholars have extensively studied SRM flux-linkage modeling using various methods, such as linearization, finite element analysis, and intelligent modeling [9, 10]. However, the inability to obtain accurate flux-linkage models continues to result in excessive torque ripple in SRM torque control systems. Given that SRMs are increasingly been applied in complex environments with multiphysical field coupling and high-precision control requirements, the demand for highly accurate flux-linkage models in SRM torque control systems has become increasingly pronounced. Addressing the limitations caused by magnetic saturation in flux-linkage modeling to achieve high-precision SRM torque ripple control has emerged as a pressing challenge. Consequently, accurately identifying the parameters of

*E-mail address: wlb1166@163.com
ISSN: 1791-2377
doi:10.25103/jestr.172.16

SRM's nonlinear flux-linkage models and enhancing model computational efficiency to suppress torque ripple in SRM systems hold significant engineering value.

To this end, this study uses a neural network to identify the parameters of the SRM's nonlinear flux-linkage exponential model. It integrates logistic mapping elements into the feedback layer of the diagonal recurrent neural network (DRNN), designs a chaotic control parameter, and establishes an identification system for chaotic diagonal recurrent neural network (CDRNN)-based nonlinear flux-linkage model. Utilizing flux-linkage, current, and angular position sample data, the parameters of the nonlinear exponential flux-linkage model are estimated to address issues of slow training speed and susceptibility to local minima in the neural network. This approach not only supports the development and optimization of SRM torque control applications but also serves as a reference for enhancing the precision of such systems.

2. State of the art

The flux-linkage of SRM, which is critical parameters affecting the rotor position and current, exhibits high nonlinearity, thus complicating the acquisition of precise SRM analytical model. Consequently, scholars worldwide have conducted in-depth studies on nonlinear modeling techniques for SRM. For instance, Song [11] utilized polynomial and piecewise functions to characterize flux-linkage properties; this process requires significantly fewer data than lookup table and neural network methods but with limited modeling precision. Liu [12] reconstructed flux-linkage characteristics for an entire cycle using a fuzzy logic system based on data from the torque equilibrium method; this method achieves high precision but without a functional expression, which is disadvantageous for controller design. Furthermore, Yang [13] represented a flux-linkage model using the Fourier series and fitted the coefficients with arctangent and exponential functions, a process that is renowned for its complexity and limited accuracy. In addition, Wang [14] proposed an approach using the mind evolutionary algorithm (MEA) to optimize the initial weights and thresholds of a backpropagation (BP) neural network; this method enhanced the network's training process to achieve higher accuracy and speed in the SRM electromagnetic model but failed to provide an analytical model. Li [15] developed a normalized flux-linkage modeling method that considers magnetic saturation and structural factors, which does not require detailed measurement or simulation data of SRM modeling; the model was validated using finite element methods, but it overlooks certain physical parameters during the linear normalization process. Aydemir [16] employed a nonlinear autoregressive network with exogenous inputs neural network (NARX NN) to estimate the phase flux-linkage of SRM; the model eliminated the issue with online phase resistance changes by estimating phase flux-linkage from real-time phase current measurements, but it could not establish a mathematical relationship for the flux-linkage. Marcelo [17] introduced a drift cancellation technique to mitigate sensor calibration and noise errors in estimating flux-linkage, validated through simulation and experimental results, but did not analyze the model's application to control techniques. Anupam [18] considered the effects of rotor pole height on air-gap permeability using a new flux-linkage calculation method that derived expressions for aligned and misaligned rotor positions based on magnetic material characteristics. However, the flux-linkage model was not been discussed. Rocca [19] used interpolation techniques based on second-order Frohlich-Kennelly equations to fit the saturated flux-linkage curve; they were been validated through finite element analysis and physical prototypes but did not provide a comprehensive flux-linkage equation.

To address the issue of excessive torque ripple during low-speed operation, Dang [20] designed a D-Sigmoid activation function to construct a neural network inductance model and introduced a torque bias preprocessing method to accelerate the correction of inductance model parameters, thereby suppressing torque ripple. However, the proposed method based on online neural network calculations involves substantial computational effort and is unsuitable for real-time SRM control. Uddin [21] divided the SRM stator teeth into saturable and nonsaturable linear segments whose thickness varies with rotor position, thus enhancing the accuracy of flux-linkage calculations but complicating calculations that are dependent on SRM's geometric shape. Meanwhile, Hao [22] proposed an air-gap flux-linkage model analysis method based on winding functions and the current distribution to predict SRM's nonlinear transient torque, which did not require initial flux-linkage data and was numerically validated using finite element methods. However, the proposed method also did not define the relationships among geometric shapes, rotor positions, and magnetic saturation. Stuikys [23] introduced a multibranch magnetic circuit calculation method using a finite element analysis of SRM geometric profiles to refine flux-linkage curves, thus effectively enhancing the estimation accuracy of flux-linkage; however, the applicability of the proposed method is limited by variations in SRM models. Li [24] analyzed phase inductance using Maxwell's equations under specific boundary conditions, a process that involves substantial engineering calculations. Cai [25] simplified the mathematical model to convert the saturated incremental inductance of an SRM into unsaturated inductance; this model reconstructs the full-cycle unsaturated inductance but overlooks specific details during dynamic changes in inductance, thus failing to reflect the strong nonlinearity of inductance fully. Li [26] presented a distribution control method, a common SRM control approach that disregards magnetic saturation and edge effects, using only a linear inductance model; it solves phase currents through a torque-current inverse model but does not consider the substantial modeling errors caused by the strong nonlinear inductance characteristics.

The aforementioned studies primarily involved the use of equivalent magnetic circuit modeling for SRM flux-linkage. On the one hand, these studies typically applied general linear and quasilinear modeling methods. These methods reduced the complexity of mathematical formula derivation and associated calculations but ignored mutual inductance effects because of changes in the relative positions of stators and rotors, which significantly deviated from actual results. On the other hand, methods based on neural networks failed to address the issue of local minima during network training, thus preventing the acquisition of precise SRM flux-linkage analytical models. This study introduces logistic mapping elements into the feedback layer of the DRNN and designs chaotic control elements. Moreover, it proposes a method based on the CDRNN for identifying parameters of the SRM nonlinear exponential flux-linkage model. Utilizing the generalization capability of the DRNN, the proposed methodological model without reliance on prior experience or theoretical knowledge. It enhances the generalization

performance of the nonlinear exponential flux-linkage analytical model and prevents the DRNN from falling into local minima, thus ensuring modeling accuracy and laying a foundation for precise SRM torque ripple control.

The remainder of this study is organized as follows. Section 3 provides a brief overview of the exponential function-based SRM nonlinear flux-linkage model by incorporating logistic mapping elements into the DRNN feedback layer, designing chaotic control parameters, and constructing a CDRNN-based exponential flux-linkage parameter identification structure. Section 4 identifies flux-linkage model parameters based on empirical SRM flux-current-angle sample data, thereby validating the accuracy of the flux-linkage model obtained. Section 5 summarizes the study by highlighting the improvements in the identification accuracy of SRM flux-linkage parameters achieved through the CDRNN identification algorithm, thus obtaining a precise SRM flux-linkage analytical model that is beneficial for the subsequent precise control of SRM torque.

3. Methodology

3.1 Exponential flux-linkage model for SRM

Based on the principles of electromechanical energy conversion, the SRM can be viewed as a two-port device consisting of one electrical port and one mechanical port. Ignoring iron losses and mutual inductance between phases, the energy conversion of the SRM is illustrated, as shown in Figure 1.

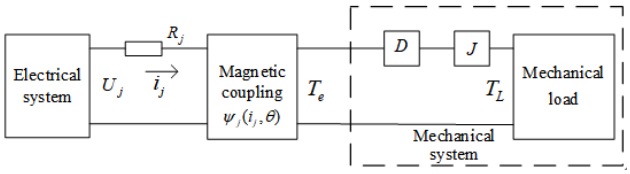

Fig. 1. Schematic diagram of electromechanical energy conversion in an SRM

Where U_j represents the voltage (V) of phase j; R_j represents the resistance (Ω) of phase j; $\psi_j(i_j,\theta)$ represents the flux-linkage linkage (Wb) of phase j; i_j represents the current (A) of phase j; θ represents the rotor's angular position (°); T_e represents the electromagnetic torque of the motor (Nm); T_L represents the load torque (Nm); D represents the coefficient of viscous friction; J represents the moment of inertia of the motor (kg/m^2).

According to the basic principles of circuitry, the voltage balance equation for phase j of the motor is given by

$$U_j = R_j i_j + \frac{d\psi_j}{dt} \tag{1}$$

The mechanical motion equation for the motor's rotor can be expressed as

$$\begin{cases} J\dfrac{d\omega}{dt} = T_e - D\cdot\omega - T_L = \sum_{j=1}^{m} T_j - D\cdot\omega - T \\ \dfrac{d\theta}{dt} = \omega \end{cases} \tag{2}$$

where ω represents the rotor's angular velocity (rad/s) and m denotes the number of phases in the motor.

The induced electromotive force at the electrical port and the electromagnetic torque at the mechanical port are coupled through the magnetic field, thus facilitating energy transfer. The electromechanical energy conversion process within a working cycle of the motor can be described by the magnetic flux-current coordinate plane. Given that the rotor of the switched reluctance motor has a salient pole structure, its flux-linkage varies not only with the current cycle but also with the rotor position cycle. Moreover, it can be described using magnetic flux-current-rotor angle coordinates. For an m-phase switched reluctance motor, ignoring mutual inductance between windings, the electromagnetic torque of the motor can be considered generated solely by a single winding, thus resulting in the electromagnetic torque for phase j of the SRM as

$$\begin{cases} T_j(\theta,i_j) = \dfrac{\partial W'_j(\theta,i_j)}{dt} \\ W'_j(\theta,i_j) = \int_0^{i_j} \psi_j(\theta,i_j)di_j \end{cases} \tag{3}$$

where $W'_j(\theta,i_j)$ represents the magnetic coenergy (J) of phase j of the motor.

As derived from Equation (3-3), the nonlinearity of electromagnetic torque is primarily due to the nonlinearity of the motor's flux-linkage linkage. Hence, the establishment of a reasonable flux-linkage model must be examined. This study utilizes an exponential function-based SRM flux-linkage model, which is presented as follows:

$$\begin{cases} \psi_j(\theta,i_j) = \psi_{sat}(1-e^{i_j f_j(\theta)}),\ j=1,2,...,m \\ f_j(\theta) = a + b\cos(N_r\theta - (j-1)2\pi/m) \end{cases} \tag{4}$$

where ψ_{sat} represents the saturation flux-linkage linkage; N_r is the number of rotor poles; a and b are coefficients of the function $f_j(\theta)$, with a > b.

By substituting Equation (4) into Equation (3), the instantaneous torque of the motor can be calculated as

$$\begin{aligned} T_e &= \sum_{j=1}^{3} T_j(\theta,i_j) = \sum_{j=1}^{3}\frac{\partial}{\partial\theta}\int_0^{i_j}\psi_{sat}(1-e^{-i_j f_j(\theta)})di_j \\ &= \sum_{j=1}^{3}\frac{\partial}{\partial\theta}[\psi_{sat}i_j - \int_0^{i_j}\psi_{sat}e^{-i_j f_j(\theta)}di_j] = \sum_{j=1}^{3}\frac{\partial}{\partial\theta}\frac{\int_0^{i_j}\psi_{sat}e^{-i_j f_j(\theta)}d(-i_j f_j(\theta))}{f_j(\theta)} \\ &= \sum_{j=1}^{3}\frac{\partial}{\partial\theta}\frac{\psi_{sat}e^{-i_j f_j(\theta)}\big|_0^{i_j}}{f_j(\theta)} = \frac{\partial}{\partial\theta}\frac{\psi_{sat}(e^{-i_j f_j(\theta)}-1)}{f_j(\theta)} \\ &= \sum_{j=1}^{3}\psi_{sat}\frac{e^{-i_j f_j(\theta)}(-i_j\frac{df_j(\theta)}{d\theta})f_j(\theta) - (e^{-i_j f_j(\theta)}-1)\frac{df_j(\theta)}{d\theta}}{f_j^2(\theta)} \\ &= \sum_{j=1}^{3}\frac{\psi_{sat}}{f_j^2(\theta)}\frac{df_j(\theta)}{d\theta}\{1-[1+i_j f_j(\theta)]e^{-i_j f_j(\theta)}\} \end{aligned} \tag{5}$$

Thus, to derive the analytical model of SRM's electromagnetic torque, the parameters ψ_{sat}, a, and b must be estimated from the flux-linkage model in Equation (4).

3.2 Principles of flux-linkage model parameter identification

The DRNN connection layer includes a feedback unit, where the output of neurons in the connection layer forms part of the

input for the next time axis, thus incorporating the load state from the previous time axis. This configuration overcomes the inability of the deep neural network (DNN) to map dynamic load characteristics fully, thus making the DRNN particularly adept at identifying the nonlinear characteristics of SRM flux-linkage models. However, similar to the DNN, the DRNN can fall into local minima traps because of their hidden layers. To overcome this issue, the CDRNN was designed to identify the parameters of the nonlinear SRM flux-linkage model. The CDRNN incorporates logistic mapping items into the DRNN feedback layer by utilizing chaotic search properties for global optimization to prevent falling into local minima.

Using the obtained SRM magnetic flux-current-angle data, the CDRNN is employed to estimate ψ_{sat}, a, and b from Equation (4). The structure for estimating the parameters of the nonlinear flux-linkage model using CDRNN is shown in Figure 2.

In the diagram, the CDRNN neural network continuously adjusts its weights based on the discrepancy between the measured flux-linkage linkage $\psi(k)$ and the calculated values from the nonlinear flux-linkage model $\psi'(k)$, as well as input data that has been delayed, such as current, angle, and flux-linkage. This adjustment continues until the error performance requirements are met, thereby estimating the parameters to be identified (ψ_{sat}, a, b). The solid and dashed arrows traversing the neural network module represent the dynamically adjusting network weights.

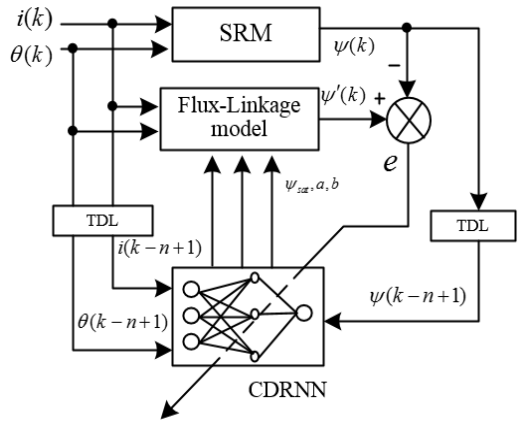

Fig. 2. Structural diagram for estimating nonlinear flux-linkage model parameters using CDRNN

3.3 CDRNN and stability analysis

The structure of the CDRNN incorporating logistic chaos mapping is shown in Figure 3.

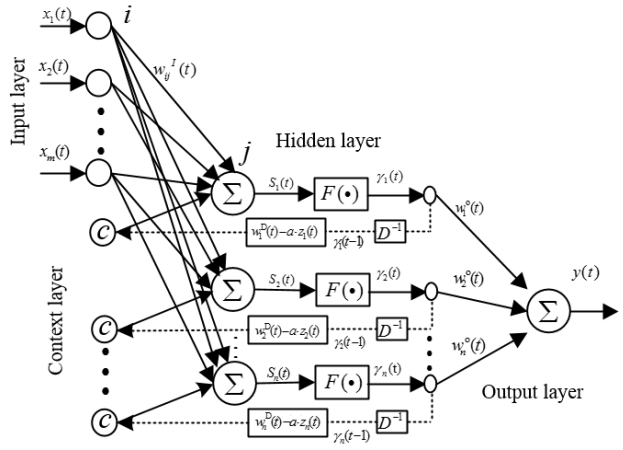

Fig. 3. Structure of the CDRNN incorporating logistic chaos mapping

As depicted, the CDRNN consists of an input layer, a hidden layer, a connection layer, and an output layer. Under the influence of logistic mapping inputs to the connection layer, chaotic motions occur in the hidden layer, thus preventing the network output from falling into local minima. The CDRNN algorithm is described by

$$\begin{cases} y(t) = W^o(t)\gamma(t) \\ \gamma(t) = F(S(t)) \\ S(t) = W^I(t)X(t) + (W^D(t) - a \cdot Z(t))\ \gamma(t\text{-}1) \\ Z(t+1) = 1 - 2 \cdot Z(t)^2 \end{cases} \tag{6}$$

where $X(t)$ is the input layer vector; $y(t)$ is the output of the CDRNN; $g(t)$ and $g(t\text{-}1)$ are the output vectors of the intermediate hidden layer and its delayed version by one sampling period, respectively; $F(\cdot)$ is the sigmoid function; $W^I(t)$, $W^D(t)$, and $W^o(t)$ are the network weights for the CDRNN's input layer, connection layer, and output layer, respectively; a is the chaos control coefficient, which ranges from 0 to 4; $Z(t)$ is the logistic mapping function.

The network output error is defined as

$$e(t) = d^* - y(t) + v(t) \tag{7}$$

where d^* is the desired network output; $v(t)$ represents the system disturbance error.

Based on the network output error, the performance index of the CDRNN identification is defined as

$$E(t) = \frac{1}{2} e(t)^2 \tag{8}$$

The weight update algorithm for the output layer of the CDRNN is designed as

$$\begin{cases} W^o(t+1) = W^o(t) - \dfrac{\mu^o(t)}{\rho^o(t)} \dfrac{\partial E(t)}{\partial W^o(t)} \\ \qquad\qquad = W^o(t) + \dfrac{\mu^o(t)}{\rho^o(t)} e(t)\gamma(t) \\ \rho^o(t) = \dfrac{1 - \|\gamma(t)\|^2}{2} \\ \mu^o(t) = \begin{cases} 1, & \|e(t)\| \geq \|\Delta^o(t)\| \\ 0, & \|e(t)\| < \|\Delta^o(t)\| \end{cases} \\ \Delta^o(t+1) = \Delta^o(t) + \dfrac{\mu^o(t)}{\rho^o(t)} \bar{e}(t) \end{cases} \tag{9}$$

where $\rho^o(t)$ represents the normalization factor for the output layer; $\mu^o(t)$ is the adaptive learning rate for the output layer; $\Delta^o(t)$ is the error control item for the output layer; $\bar{e}(t) = [|e_1(t)|, |e_2(t)|, ..., |e_h(t)|]^T$ is the network output error vector.

The hidden layer network weight update algorithm for the CDRNN is given by

$$\begin{cases} W^I(t+1) = W^I(t) - \dfrac{\mu^I(t)}{\rho^I(t)} \dfrac{\partial E(t)}{\partial W^I(t)} \\ \quad = W^I(t) - \dfrac{\mu^I(t)}{\rho^I(t)} \dfrac{\partial E(t)}{\partial \gamma(t)} \dfrac{\partial \gamma(t)}{\partial F(t)} \dfrac{\partial F(t)}{\partial W^I(t)} \\ \quad = W^I(t) + \dfrac{\mu^I(t)}{\rho^I(t)} e(t) W^o(t) F'(t) X(t) \\ \rho^I(t) = \dfrac{1 - \left\| W^o(t) F'(t) X(t) \right\|^2}{2F'_{\min}(t)} \\ \mu^I(t) = \begin{cases} 1, & \|e(t)\| \geq \|\Delta^I(t)\| \\ 0, & \|e(t)\| < \|\Delta^I(t)\| \end{cases} \\ \Delta^I(t+1) = \Delta^I(t) + \dfrac{\mu^I(t)}{\rho^I(t)} \bar{e}(t) \end{cases} \tag{10}$$

where $F'_{\min}(t)$=min($F'(t)$)≠0, where t denotes time; $\rho^I(t)$ is the normalization coefficient for the hidden layer; $\mu^I(t)$ is the adaptive learning rate for the hidden layer; $\Delta^I(t)$ is the error control item for the hidden layer.

The input layer network weight update algorithm for the CDRNN is structured as

$$\begin{cases} W^D(t+1) = W^D(t) - \dfrac{\mu^D(t)}{\rho^D(t)} \dfrac{\partial E(t)}{\partial W^D(t)} \\ \quad = W^D(t) - \dfrac{\mu^D(t)}{\rho^D(t)} \dfrac{\partial E(t)}{\partial \gamma(t)} \dfrac{\partial \gamma(t)}{\partial F(t)} \dfrac{\partial F(t)}{\partial W^D(t)} \\ \quad = W^D(t) + \dfrac{\mu^D(t)}{\rho^D(t)} e(t) W^o(t) F'(t) \gamma(t-1) \\ \rho^D(t) = \dfrac{1 - \left\| W^o(t) F'(t) \gamma(t-1) \right\|^2}{2F'_{\min}(t)} \\ \mu^D(t) = \begin{cases} 1, & \|e(t)\| \geq \|\Delta^D(t)\| \\ 0, & \|e(t)\| < \|\Delta^D(t)\| \end{cases} \\ \Delta^D(t+1) = \Delta^D(t) + \dfrac{\mu^D(t)}{\rho^D(t)} \bar{e}(t) \end{cases} \tag{11}$$

where $\rho^D(t)$ represents the normalization coefficient for the input layer; $\mu^D(t)$ is the adaptive learning rate for the input layer; $\Delta^D(t)$ is the error control item for the input layer.

Note: The excitation function of the hidden layer is $F(s(t))=1/(1+\exp(-s(t)))$, and its derivative $0 < F'(s(t)) < 1$ is positive. According to the characteristics of neural networks, the weights for the input, hidden, and output layers are all within the range of 0 to 1. Therefore, the normalization coefficients $r^o(t)$, $r^I(t)$, and $r^D(t)$ are all positive.

4. Result Analysis and Discussion

To estimate the three parameters to be identified in the flux-linkage model, sample data of flux, current, and angle for the SRM must be obtained. As shown in Figure 4, the principle of flux-linkage detection for a single phase of the SRM assumes identical winding parameters per phase and disregards mutual inductance between phases. The SRM is fixed to the base of the test rig with an indexing plate, which allows the adjustment of the rotor's positional angle by manipulating the indexing plate's handle. The host computer uses the Real-Time module in MATLAB/Simulink and a PCI interface data acquisition card for data communication, thus controlling the switching of power tubes for the phase windings and collecting voltage and current data.

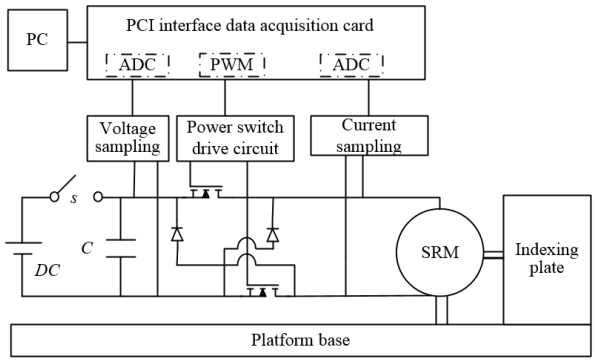

Fig. 4. Schematic diagram of flux-linkage eetection for SRM phase windings

The SRM flux-linkage measurement system is shown in Figure 5. The flux-linkage detection of the SRM utilizes a step voltage method where a step voltage is applied to the motor's phase winding when the initial flux-linkage is zero. This process involves the real-time monitoring of voltage and current and uses Euler's method for numerical integration to calculate flux-linkage. During the flux test, the rotor's positional angle is fixed because the designed SRM is a three-phase 12/8 structure with a rotor angle period of 45°. Given that the phase winding's flux-linkage is symmetric within one period, flux-linkage data can be sufficiently collected from 0° to 22.5°. Therefore, the angle at which the flux-linkage reaches its maximum within an angle period, which is when the salient poles of the stator and rotor align, is defined as 22.5°. A PWM generator is designed using MATLAB/Simulink to control the opening of power tubes and simultaneously collect voltage and current data from the phase windings. After a sampling session ends, the PWM generator stops, the power tubes are turned off, and Simulink saves the collected voltage and current data to the MATLAB workspace. To ensure that the initial value of flux-linkage is zero for digital integration, the circuit's switch is disconnected after sampling. Once the winding has fully discharged, the next data sampling occurs. The rotor angle is sampled at 1.5° intervals, thereby obtaining 16 sets of data.

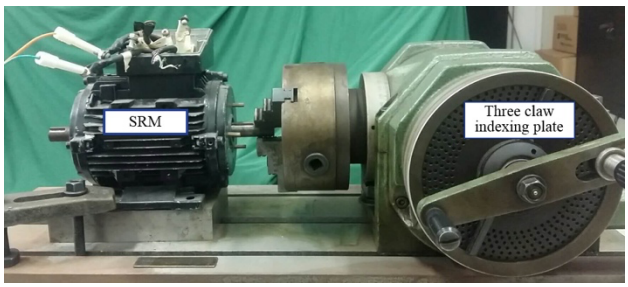

Fig. 5. SRM Flux-Linkage Measurement Experimental System

A model for identifying nonlinear flux-linkage parameters using CDRNN based on Figure 2 is established in MATLAB/Simulink. It utilizes the experimentally obtained flux-current-angle data to identify the parameters ψ_{sat}, a, and b. Figure 6 illustrates the changes in parameters during the CDRNN identification process. As shown, the performance error of the CDRNN eventually converges to zero, thus indicating stability throughout the identification process. At the start of identification, to avoid falling into local minima

due to significant errors, chaotic control parameter a is used to induce chaotic behavior in the network by utilizing its chaotic ergodicity for optimization. Once the performance error falls within the set desired range, the chaotic control parameter is turned off to accelerate the convergence of the identification process. The learning rates for the input, hidden, and output layers of the CDRNN are dynamically adjusted, thus indicating that the designed neural network can adaptively change based on the error control items set for each layer. Hence, the network's generalization capability is effectively enhanced. The results demonstrate that the proposed CDRNN can autonomously modulate chaos, thus significantly improving the network's convergence speed and generalization performance.

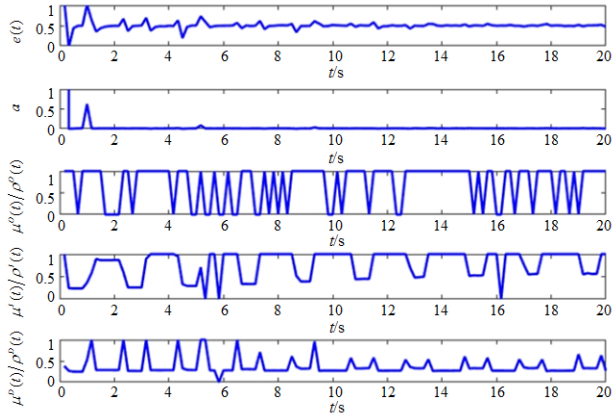

Fig. 6. Changes in parameters during the CDRNN identification process

Figure 7 presents the results of the parameter identification of the flux-linkage model. At the start of the identification, given the significant initial errors, the network is made to enter a chaotic state by adjusting the logistics control parameter a. It utilizes the chaotic ergodicity to search globally for optimal points, which effectively prevents the network from getting stuck in local minima. Approximately one second into the operation, when the network performance error reaches the preset desired value, the chaotic control parameter is automatically turned off. This setting allows the parameter identification to enter a converging state in less than two seconds, thus effectively accelerating the convergence of the identification process. By averaging the steady-state portion of the identified parameters, the flux-linkage model parameters are estimated to be $\psi_{sat} = 0.1597$, $a = 0.0297$, and $b = -0.0057$.

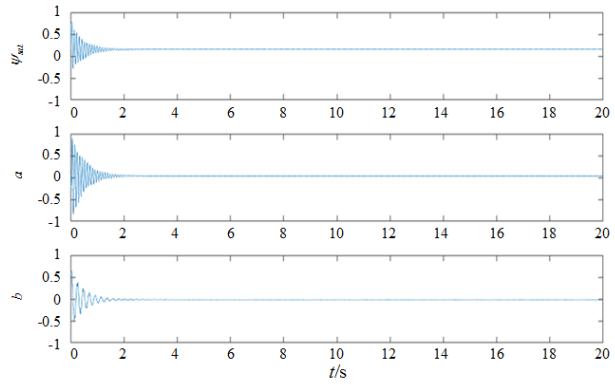

Fig. 7. Results of flux-linkage model parameter identification

Angles and currents were input into the flux-linkage model at intervals of 0.5° and 0.5A, respectively, to obtain the corresponding fluxes. The flux-current-angle surface, as shown in Figure 8, transitions smoothly and is continuous without any breaks within the range of inputs. Thus, it accurately reflects the variations in flux-linkage with respect to angle and current.

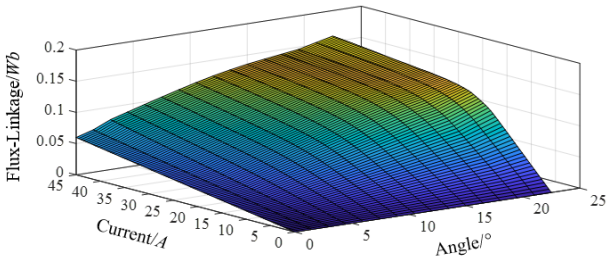

Fig. 8. Flux-current-angle surface

To verify the effectiveness of the model parameters identified by the CDRNN, the flux-linkage obtained from the CDRNN identification model was compared with the flux-linkage measured experimentally, and a flux-linkage error surface was plotted. Figure 9 shows the flux-current-angle error surface, where the maximum flux-linkage error does not exceed 0.01 Wb, the maximum flux-linkage is 0.2 Wb, and the accuracy is 95%. This outcome demonstrates that the proposed flux-linkage analytical model has high precision.

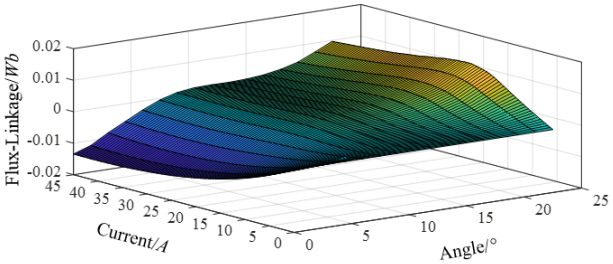

Fig. 9. Flux-current-angle error surface

To validate further the accuracy of the flux-linkage curves identified using the CDRNN-based parameter identification method proposed in this study, the flux-linkage calculations under varying currents were performed at stator and rotor pole positions of 10.5° and 19.5°, respectively. Then, they were compared with DRNN estimated data and experimental data. As shown in Figures 10 and 11, the results indicate that at lower currents (0-10A), the flux-linkage calculations obtained through CDRNN identification closely match the experimental data, whereas the DRNN-identified flux-linkage begins to show significant errors starting from 5A. As the current increases, the errors in flux-linkage calculations using CDRNN are noticeably smaller than those using DRNN, thus demonstrating higher model accuracy.

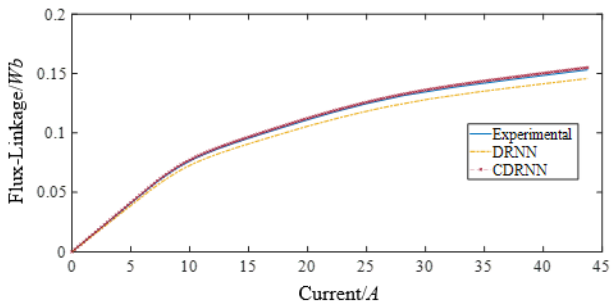

Fig. 10. Comparison of flux-linkage curves at a fixed position of 10.5°

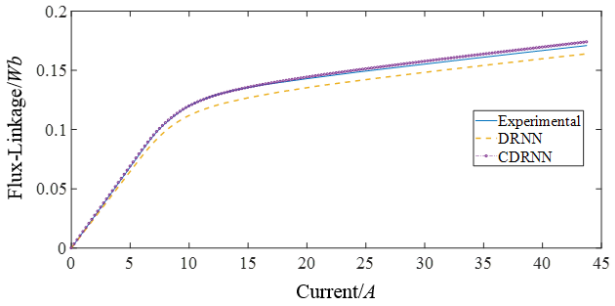

Fig. 11 Comparison of flux-linkage curves at a fixed position of 19.5°

5. Conclusions

In response to the challenges of high saturation, strong nonlinearity, and strong coupling in SRM magnetic circuits, this study introduced a CDRNN featuring a feedback layer with logistics mapping items. A control model for identifying the nonlinear flux-linkage model of SRM based on the CDRNN was established, and parameters of the flux-linkage nonlinear model were identified using SRM flux-current-angle sample data. The following conclusions could be drawn:

(1) The inclusion of logistic mapping and chaotic control parameters in the DRNN's feedback layer can prevent the standard DRNN from falling into local minima, thus ensuring convergence of the identification process.

(2) Compared with experimentally measured flux-linkage, the flux-linkage identified by the CDRNN had a maximum error of no more than 0.01 *Wb* and a maximum flux of 0.2 *Wb*, thus achieving an accuracy of 95%.

(3) Flux-linkage identified by DRNN exhibited significant errors starting at a current of 5A. As the current increased, the CDRNN provided notably smaller errors in flux-linkage calculations, thus resulting in enhanced model accuracy.

This study designed a control system for identifying parameters of the SRM nonlinear flux-linkage model based on the CDRNN, thus obtaining a relatively accurate SRM nonlinear flux-linkage model. This model has practical significance for improving precise torque control in SRM. Given the lack of a related test platform for SRM torque control, the obtained flux-linkage model could not be verified through experiments. Therefore, future work will involve conducting SRM torque control experiments and refining the nonlinear flux-linkage model to understand the nonlinear characteristics of SRM magnetic circuits more accurately.

Acknowledgements
This work was supported by the Natural Science Foundation of Zhejiang Province, China (Grant No. LTY20E050002).

References

[1] H. Chen, R. Nie, J. Gu, S. Yan, and R. Zhao, "Efficiency optimization strategy for switched reluctance generator system with position sensorless control," *IEEE-ASME T. Mech.*, vol. 26, no. 1, pp. 469-479, Feb. 2021.

[2] N. Chen, G. Z. Cao, S.D. Huang, and J. D. Sun, "Sensorless control of planar switched reluctance motors based on voltage injection combined with core-loss calculation," *IEEE Trans. Ind. Electron.*, vol. 67, no. 7, pp. 6031-6042, Jul. 2020.

[3] X.Q. Guo, S.G. Zeng, M. Wu, R. Zhong, and W. Hua, "A low-speed position sensorless scheme from standstill for low-cost SRM drives based on triple current slope difference threshold," *IEEE Trans. Ind. Electron.*, vol. 71, no. 4, pp. 3296-3306, Apr. 2024.

[4] X. Q. Guo, S. G. Zeng, R. Zhong, and W. Hua, "Automatic offline measurement of full-cycle unsaturated inductance for low-speed rotor position estimation in switched reluctance machines," *IEEE J. Em. Sel. Top. P.*, vol. 12, no. 1, pp. 849-861, Feb. 2024.

[5] A. A. Memon, S. S. H. Bukhari, and C. Hao, "Switched reluctance motoring and generating operation in single pulse, current chopping and voltage PWM modes," *Electr. Eng.*, vol. 105, no. 5, pp. 2817–2823, Oct. 2023.

[6] X. P. Cui, J. B. Sun, C. Gan, C. L. Gu, and Z. W. Zhang, "Optimal design of saturated switched reluctance machine for low speed electric vehicles by subset quasi-orthogonal algorithm," *IEEE Access*, vol. 7, pp. 101086-101095, 2019.

[7] S. J. Song, G. L. Fang, Z. H. Zhang, R. Q. Ma, and W. G. Liu, "Unsaturated inductance based instantaneous torque online estimation of switched reluctance machine with locally linearized energy conversion loop," *IEEE Trans. Ind. Electron.*, vol. 65, no. 8, pp. 6109-6119, Aug. 2018.

[8] L. F. Ge, Z. Z. Fan, N. Du, J. L. Huang, D. X. Xiao, and S. J. Song, "Model predictive torque and force control for switched reluctance machines based on online optimal sharing function," *IEEE Trans. Power Electron.*, vol. 38, no. 10, pp. 12359-12364, Oct. 2023.

[9] Z. Djelloul-Khedda, K. Boughrara, F. Dubas, and R. Ibtiouen, "Nonlinear analytical prediction of magnetic field and electromagnetic performances in switched reluctance machines," *IEEE Trans. Magn.*, vol. 53, no. 7, pp. 1-11, Jul. 2017.

[10] L. F. Ge, I. Ralev, A. Klein-Hessling, S. J. Song, and R. De Doncker, "A simple reluctance calibration strategy to obtain the flux-linkage characteristics of switched reluctance machines," *IEEE Trans. Power Electron.*, vol. 35, no. 3, pp. 2787-2798, Mar. 2020.

[11] S. J. Song, M. Zhang, and L. F. Ge, "A new fast method for obtaining flux-linkage characteristics of SRM," *IEEE Trans. Ind. Electron.*, vol. 62, no. 7, pp. 4105-4117, Jul. 2015.

[12] J. Liu, G. F. Wang, S. Li, D. Liu, and Y. S. Fan, "A novel method to obtain the flux-linkage characteristics of switched reluctance motors," *IEEE Trans. Magn.*, vol. 57, no. 11, pp. 1-11, Nov. 2021.

[13] W. H. Yang, B. Gou, Y. Lei, X. X. Song, and J. Wang, "SRM torque ripple suppression method based on model predictive control," *Adv. Technol. Electr. Eng. Energy*, vol. 39, no. 8, pp. 18-28, Sep. 2020.

[14] C. M. Wang, A.Y. Wang, X. D. Yao, S. X. Yin, and J. C. Li, "Modeling of static electromagnetic characteristics of switched reluctance motor based on MEA-BP Neural Network," *Electr. Mach. Ctrl. Appl.*, vol. 49, no. 5, pp. 64-68, Aug. 2022.

[15] Y.Q. Li, Q. S. Ma, and P. Xu, "Improved general modelling method of SRMs based on normalised flux linkage," *IET Electr. Power Appl.*, vol. 14, no. 2, pp. 316-324, Feb. 2020.

[16] M. Aydemir and H. I. Okumus, "Phase flux linkage estimation of external rotor switched reluctance motor with NARX neural network," *Electr. Eng.*, vol. 105, no. 2, pp. 1223-1233, Apr. 2023.

[17] V. D. P. Marcelo and A. D. S. B. Tárcio, "A new flux linkage estimation with drift cancellation technique for switched reluctance machines," *Electronics*, vol. 9, no. 3, pp. 9030405, Feb. 2020.

[18] A. Verma, S. S. Ahmad, and G. Narayanan, "Analytical prediction of static flux-linkage characteristics of switched reluctance machine," *IEEE Trans. Ind. Appl.*, vol. 59, no. 5, pp. 5886-5899, Sep. 2023.

[19] R. Rocca, G. De Donato, P. Bolognesi, C. Boccaletti, and F. G. Capponi, "Improved design-oriented analytical modelling of switched reluctance machines based on fröhlich-kennelly equations," *IEEE Trans. Energy Convers.*, vol. 39, no. 1, pp. 734-746, Mar. 2024.

[20] X. J. Dang and Y. X. Li, "Construction of neural network inductance model based on mechanism characteristics and SRM torque ripple suppression control," *Micromotors*, vol. 55, no. 9, pp. 39-44+63, Sep. 2022.

[21] W. Uddin and Y. Sozer, "Analytical modeling of mutually coupled switched reluctance machines under saturation based on design geometry," *IEEE Trans. Ind. Appl.*, vol. 53, no. 5, pp. 4431-4440, Sep. 2017.

[22] H. Hua and W. Hua, "Analytical prediction of torque of switched reluctance machines considering nonlinear characteristics," *IEEE Trans. Ind. Electron.*, vol. 69, no. 1, pp. 190-201, Jan. 2022.

[23] A. Stuikys and J. Stuikys, "Rapid multi-objective design optimization of switched reluctance motors exploiting magnetic flux tubes," *IET Sci. Meas. Technol.*, vol. 12, no. 2, pp. 223-229, Mar. 2018.

[24] S. F. Li, Z. Shen, C. Gong, T. G. Habetler, and R. G. Harley, "An enhanced analytical calculation of the phase inductance of switched reluctance Machines," *IEEE Trans. Ind. Appl.*, vol. 55, no. 2, pp. 1392-1407, Mar. 2019.

[25] J. Cai and Z. Y. Liu, "An unsaturated inductance reconstruction based universal sensorless starting control scheme for SRM drives," *IEEE Trans. Ind. Electron.*, vol. 67, no. 11, pp. 9083-9092, Nov. 2020.

[26] H. D. Li, B. Bilgin, and A. Emadi, "An improved torque sharing function for torque ripple reduction in switched reluctance machines," *IEEE Trans. Power Electron.*, vol. 34, no. 2, pp. 1635-1644, Feb. 2019.